Supporting Materials

Graphene Oxide/Chitosan/Calcium Silicate Aerogels for Hemostasis and Infectious Wound Healing

Jianmin Xue [1,2,†], Yi Zheng [1,2,†], Zhibo Yang [1,2], Jinzhou Huang [1,2], Wenping Ma [1,2], Zhiguang Huan [1,2], Yufang Zhu [1,2,*] and Chengtie Wu [1,2,*]

[1] State Key Laboratory of High Performance Ceramics and Superfine Microstruture, Shanghai Institute of Ceramics, Chinese Academy of Sciences, Shanghai 200050, China
[2] Center of Materials Science and Optoelectronics Engineering, University of Chinese Academy of Sciences, Beijing 100049, China
* Correspondence: zjf2412@163.com (Y.Z.); chengtiewu@mail.sic.ac.cn (C.W.)
† These authors contributed equally to this work.

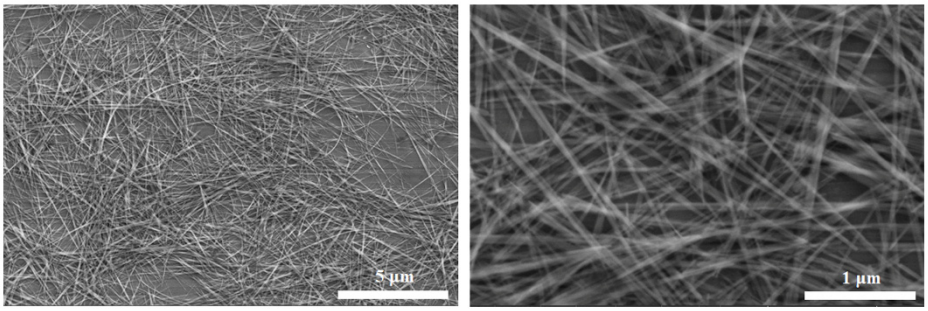

Figure S1. The morphology of calcium silicate hydrate nanofibers. The calcium silicate hydrate nanofibers were successfully synthesized through hydrothermal method.

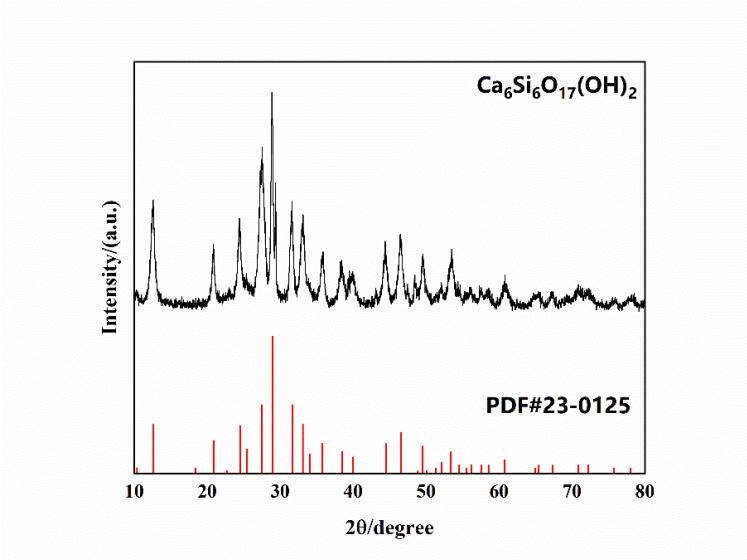

Figure S2. The XRD pattern of calcium silicate hydrate nanofibers. The phase calcium silicate hydrate nanofibers was $Ca_6Si_6O_{17}(OH)_2$.

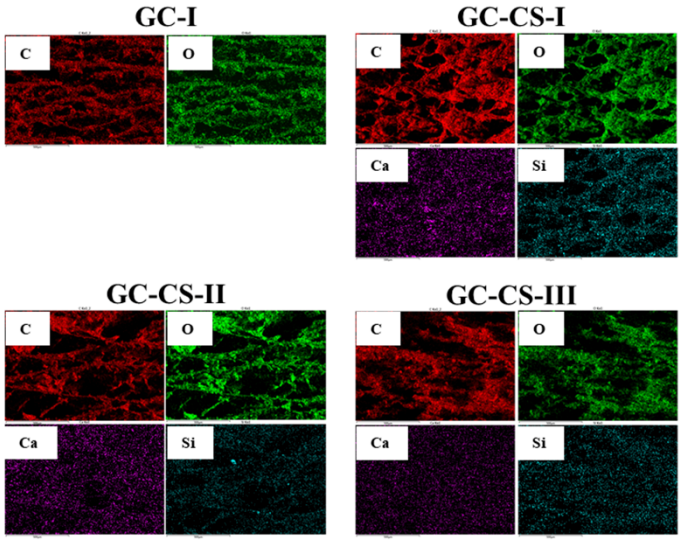

Figure S3. The EDS mapping of different GC-CS aerogels. The EDS mapping confirmed the calcium and silicon elements were successfully incorporated into GC-CS aerogels.

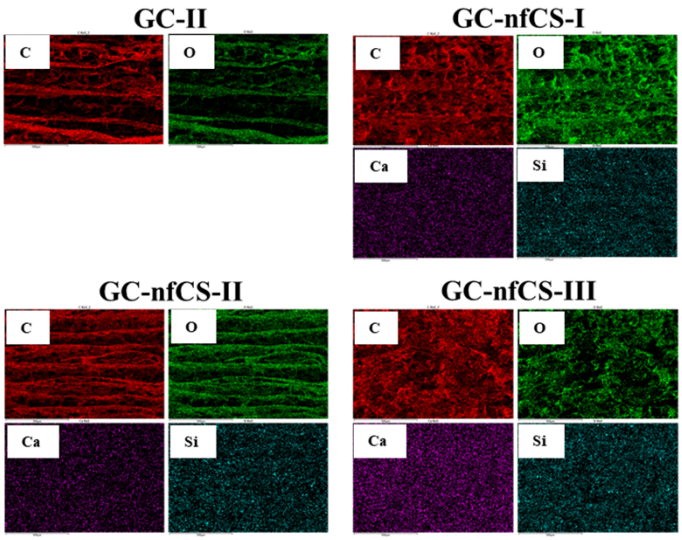

Figure S4. The EDS mapping of different GC-CS aerogels**.** The EDS mapping showed the calcium silicate hydrate nanofibers were successfully mixed with other components in GC-nfCS aerogels.

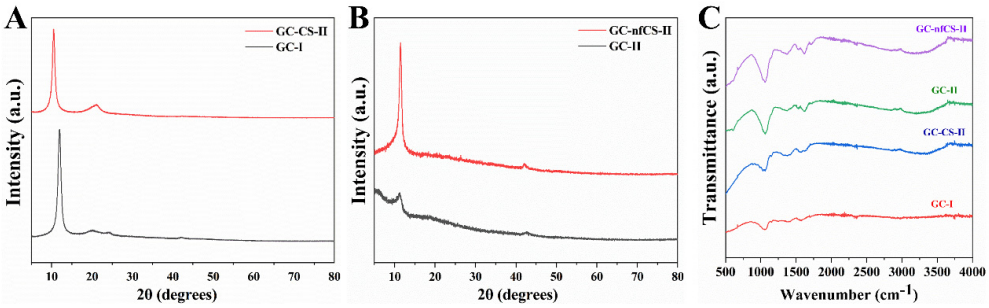

Figure S5. The XRD and FTIR of different materials. (A) The XRD patterns of GC-I and GC-CS-II aerogels. (B) The XRD patterns of GC-II and GC-nfCS-II aerogels. (C) The FTIR spectra of GC-I, GC-CS-II, GC-II and GC-nfCS-II aerogels.

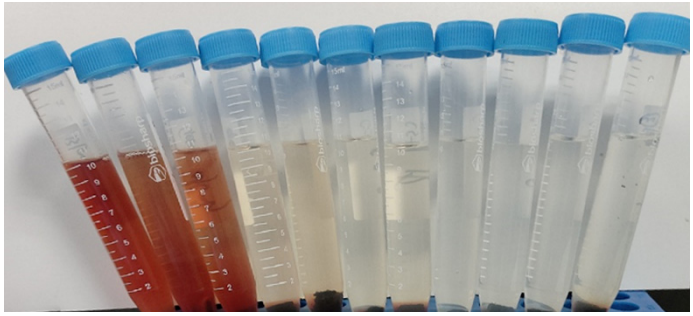

Figure S6. The photographs of different groups after BCI tests**.** The GC-CS and GC-nfCS groups obviously possessed more clear solutions after BCI tests, reflecting their lower BCI values and better blood coagulation capacity (From left to right: Blank, Gauze, Gelatin sponge. GC-I, GC-CS-I, GC-CS-II, GC-CS-III, GC-II, GC-nfCS-I, GC-nfCS-II and GC-nfCS-III).

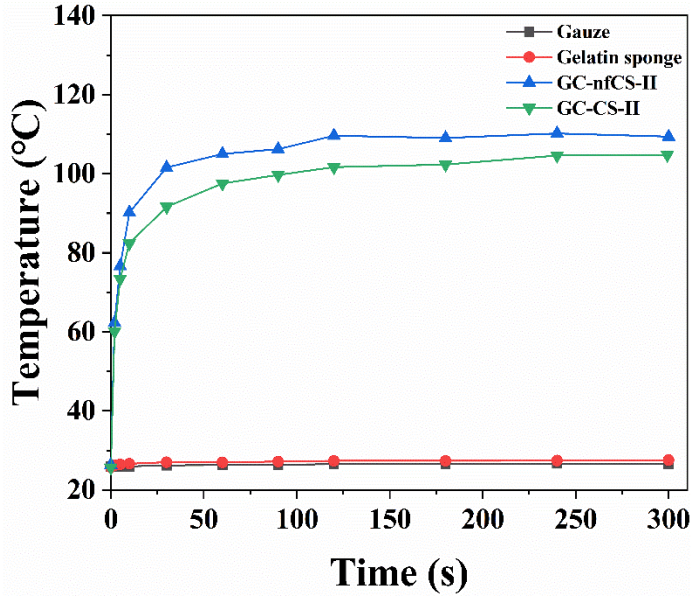

Figure S7. The *in vitro* photothermal performance of different materials. The temperatures of gauze and gelatin sponge had no obvious change under laser irradiation, while GC-CS-II and GC-nfCS-II aerogels possessed good photothermal effect.

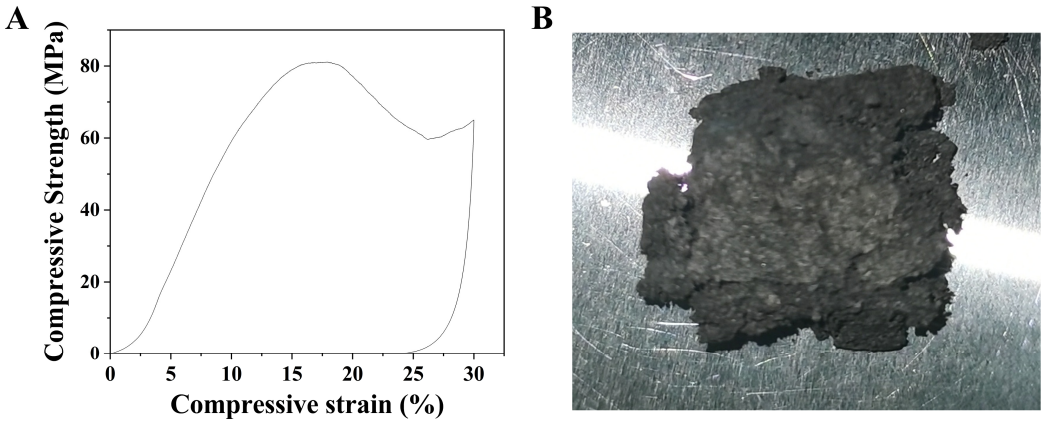

Figure S8. The compressive properties of GC-CS-II-disorder aerogel. (A) The stress-strain curves of GC-CS-II-disorder aerogel with compressive strain of 30%. (B) The photograph of GC-CS-II-disorder aerogel after compressive test.

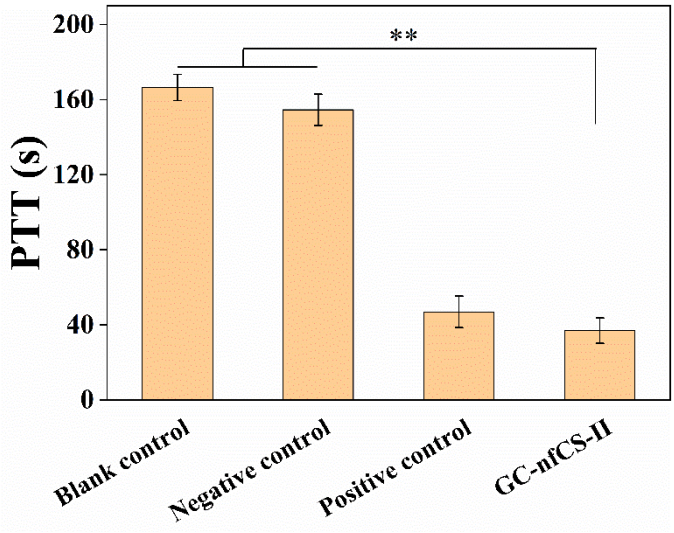

Figure S9. PTT of GC-CS-II aerogel. The PTT of GC-nfCS-II was significantly lower than those of blank control and negative control, demonstrating that GC-nfCS-II could activate the intrinsic pathway of coagulation.

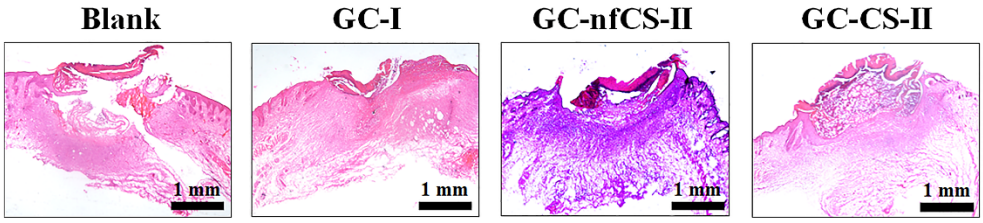

Figure S10. HE staining images of different groups for 7 days. At day 7, the GC-CS-II and GC-nfCs-II groups showed closed wounds with scab.

Table S1. The constituent contents of different aerogels.

Aerogels	$W_{Graphene\ oxide}$: $W_{Chitosan}$: $W_{Bioactive\ component}$
GC-I	50:30:0
GC-CS-I	30:50:20
GC-CS-II	50:30:20
GC-CS-III	70:10:20
GC-II	70:30:0
GC-nfCS-I	70:30:5
GC-nfCS-II	70:30:10
GC-nfCS-III	70:30:15